Jamming, Yielding, and Rheology of Weakly Vibrated Granular Media

Joshua A. Dijksman,[1,2] Geert H. Wortel,[1] Louwrens T. H. van Dellen,[1] Olivier Dauchot,[3] and Martin van Hecke[1]

[1]*Kamerlingh Onnes Lab, Universiteit Leiden, Postbus 9504, 2300 RA Leiden, The Netherlands*

[2]*Department of Physics, Duke University, Science Drive, Durham, North Carolina 27708-0305, USA*

[3]*CEA-Saclay, SPEC-GIT, URA 2464, 91191 Gif-sur-Yvette, France*

(Received 14 June 2011; published 1 September 2011)

We establish that the rheological curve of dry granular media is nonmonotonic, both in the presence and absence of external mechanical agitations. In the presence of weak vibrations, the nonmonotonic flow curves govern a hysteretic transition between slow but steady and fast, inertial flows. In the absence of vibrations, the nonmonotonic flow curve governs the yielding behavior of granular media. Finally, we show that nonmonotonic flow curves can be seen in at least two different flow geometries and for several granular materials.

DOI: 10.1103/PhysRevLett.107.108303 PACS numbers: 83.80.Fg, 45.70.−n, 83.60.La

Granular media are collections of macroscopic and athermal grains which interact through dissipative, frictional contact forces and that jam in metastable configurations [1–4]. Under sufficient shear stress, or when mechanically agitated, granular media yield and flow [5–11]. Here we ask the following: what is the rheological scenario that connects these observations?

The classical example of a inclined layer of sand illustrates that granular media exhibit a finite flow threshold, and once the material yields, the flow rate jumps to a finite value [1,3,4,12]. The simplest flow scenario that captures this behavior is sketched in Fig. 1(a), where in analogy to static and dynamic friction, the static yield stress σ_s is assumed to be larger than the dynamic yield stress σ_d.

Such scenario implies that the flow rate continuously decreases to zero when the stress (inclination angle) is lowered, as can be seen from following the flow curve in Fig. 1(a). In experiments, however, the flow is found to stop discontinuously: stress-controlled granular flows have a minimal flow rate [13–15]. This calls for a more elaborate flow curve than the one in Fig. 1(a). We sketch one that was proposed earlier [13,16] in Fig. 1(b), where the negative slope, signaling an instability, leads to a ''forbidden'' range of flow rates—when the stress is lowered below $\sigma_{\min}$, the flow rate jumps to zero [13,16].

In this Letter, we firmly establish the existence of nonmonotonic flow curves for granular media by probing their rheology, both in the presence and absence of externally supplied vibrations of strength Γ. In the absence of vibrations ($\Gamma = 0$), the flow curves indeed are of the form as sketched in Fig. 1(b), i.e., with a finite yield stress, and a dip at intermediate flow rates. As we will see, the rheology at $\Gamma = 0$ can be seen as a limiting case of the more general rheology at finite vibration strength. For $\Gamma > 0$ we find flow curves as sketched in Fig. 1(c), i.e., without a clear yield stress and with two competing branches of positive slope. This lower branch is consistent with recent experiments which have found that external agitations decrease or even quash the yield stress of granular materials [5–11], allowing for very slow flows under constant, small, stresses and finite vibration strength. Nonmonotonic flow curves such as depicted in Fig. 1(c) are well known to arise for polymer melts, micelles, and viscous suspensions [13,17–19] but have not been observed, to the best of our knowledge, for dry granular media.

The nonmonotonic flow curves are obtained in experiments with controlled flow rates, and negative slopes are expected to cause instabilities and hysteresis when the stress is controlled [19]. For $0 < \Gamma \lesssim 1$, we find that stress sweeps through the unstable regime lead to a concomitant hysteretic transition of the flow rate between the two stable branches. For $\Gamma = 0$, we find that stress-controlled yielding, i.e., the hysteretic transition from zero flow to finite flow rate, is intimately connected to the dip in the $\Gamma = 0$ flow curve. We finally show that nonmonotonic flow curves such as in Fig. 1(b) can be seen independent of flow geometry and for several, but not all, granular materials. Our findings of the robust connection between nonmonotonic flow curves and rheological instabilities shine new light on the nature of the granular jamming and yielding transitions.

Setup.—Our experiments are carried out in a split-bottom shear cell (Fig. 2), in which a layer of glass beads (diameter 1–1.3 mm) of depth $H = 18$ mm is driven by the

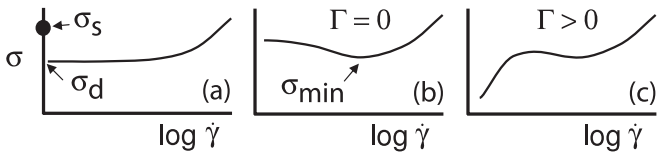

FIG. 1. Hypothetical flow curves for granular media, relating strain rate $\dot{\gamma}$ and stress σ. (a) Monotonic flow curve with a different static (σ_s) and dynamic (σ_d) yield stress. (b) Nonmonotonic flow curve—the region with negative slope signals ''forbidden'' strain rates in stress-controlled experiments. (c) A typical flow curve observed in our experiments for finite vibration strengths.

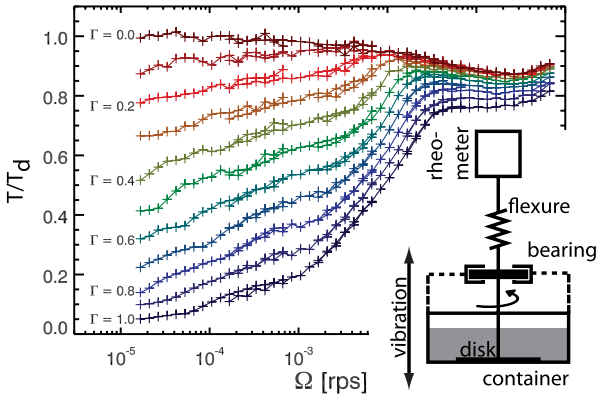

FIG. 2 (color online). Flow curves $T(\Omega)$ for $\Gamma = 0, 0.1, \ldots, 1$ as indicated. We normalize T by the dynamic yield torque T_d. Inset: vibrated split-bottom rheological setup.

rotation of a rough disk of radius $R_s = 4$ cm mounted flush with the bottom. This flow geometry has been studied extensively and produces smooth, robust, and well-controlled granular flows [20–22].

An important novel aspect of our setup is that the shear cell can be vibrated vertically and sinusoidally (distortion $<1\%$) with frequency f and amplitude A. We fix $f = 63$ Hz in the middle of a frequency window where no mechanical resonances arise. Strictly vertical vibration is ensured by guiding the motion of the shear cell with a leveled square air bearing (4 in. $\times$ 4 in., New Way) which is coupled to an electromagnetic shaker (VTS systems VG100). We control the dimensionless shaking strength, defined as $\Gamma := A(2\pi f)^2/g$, with a feedback loop to within $<10^{-3}$.

We also control the rotation rate Ω and applied torque T by a rheometer (Anton Paar DSR 301), which is coupled to the vibrating cell by means of a flexure with a torsional spring constant of 4 N m/rad and compressional spring constant of 5×10^2 N/m. We perform rheological experiments at fixed Γ and either control the torque T and measure the resulting rotation rate Ω or vice versa. All flow experiments are preceded by appropriate preshear. Disk rotation is always continuous; stick slip is not observed. Note that, as in other flow geometries, the local strain rate and stress in the split-bottom cell vary throughout the cell [23]. We thus probe the grain rheology with T as a proxy for the stress σ, and Ω as a proxy for the strain rate [14,22]. Hence, the experimentally observed curves for $T(\Omega)$ are best thought of as global flow curves.

Main phenomenology: flow curves.—Figure 2 shows the flow curves $T(\Omega)$, determined in experiments in which the rotation rate Ω is controlled, and the average torque T is measured (after removing transients).

The flow curve for $\Gamma = 0$ is nonmonotonic. For small flow rates ($\Omega < 10^{-3}$ rad/s), the stress reaches a plateau from which we determine the dynamical yield torque T_d as 13.9 ± 0.1 mN m—this value is set by the geometry [20] and the effective friction coefficient of the grains. For increasing Ω, T decreases until it reaches a minimum torque $T_{\min}$ of about 12.1 ± 0.1 mN m at $\Omega \approx 0.3$ rps. This nonmonotonic effect is substantial in magnitude and has not been observed for granular flows before. Around the minimum, the inertial number near the split is of order one, and we associate the increase of torque for larger rates with the onset of inertial flows [3,4].

The flow curves for $\Gamma > 0$ exhibit similarly nonmonotonic behavior, but differ for small Ω. As shown in Fig. 2, the range of flow rates over which the flow curves have a negative slope becomes smaller for larger Γ. At the lower Ω range of this regime, $T(\Omega)$ reaches a local maximum and for even smaller $\Omega \lesssim 0.02$ rps, we observe a decrease of T with Ω as $T \sim \log(\Omega)$. In additional experiments at fixed T we have carefully checked that the flow is stable and steady in this positive slope regime. This regime only exists for finite agitation strength and signals a novel flow regime of mechanically agitated granular flows which is unique to $\Gamma > 0$, as suggested in Fig. 1(c).

We conclude that our flow curves are consistent with the flow scenarios depicted in Figs. 1(b) and 1(c). In other systems with nonmonotonic flow curves, fixing the flow rate in the negative-slope regime typically leads to a separation of the system into two regimes, one with low, and one with large strain rate: in other words, shear banding [19]. In contrast, we have not seen any clear evidence for such behavior in our system—the flow profiles as observed at the free surface do not appear to change when we fix the flow rate in the negative-slope regime. We note that the standard shear banding mechanism depends on the shear stresses being sufficiently homogeneous, while in our system we have a strongly inhomogeneous stress field emanating from the split in the bottom [23]—this inhomogeneity is crucial in obtaining a smooth granular flow, but may hinder the observation of additional shear banding. Our setup does not allow us to determine whether dilatancy plays a significant role in the development of the nonmonotonic flow curves. Yet, since we only consider slow steady flows, the usual inertial and transient dilatancy effects [4,24] are certainly ruled out.

Rheological instability for $\Gamma > 0$.—We now turn our attention to torque-controlled experiments, and will probe whether the negative sloped regime of the flow curves for $\Gamma > 0$ leads to hysteresis. To do so, we slowly ramp T/T_d up and down between 0.8 and 1.1, i.e., through the multivalued regime. Figure 3(a) illustrates the resulting hysteresis loops. Ramping upwards, we observe a sudden jump from the slow, mechanically agitated flow branch to the rapid, inertial branch. Ramping downwards makes the flow rate jump back to the slow, mechanically agitated branch—there is considerable hysteresis between the stresses where these jumps happen. For smaller Γ, the gap between slow and rapid flow rates increases, consistent with the flow curves shown in Fig. 2.

In Fig. 3(b) we further strengthen the direct connection between the negative slope of the $T(\Omega)$ curve and the

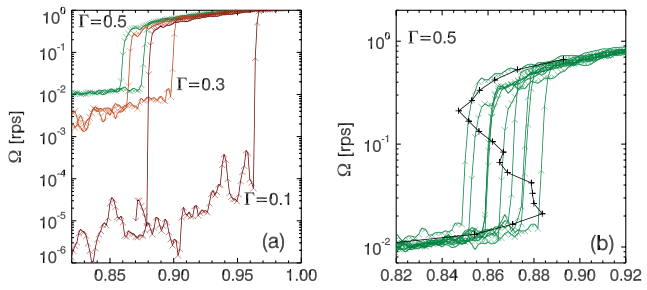

FIG. 3 (color online). (a) Finite Γ hysteresis loops for Γ = 0.1, 0.3, 0.5. (b) Several hysteresis loops at Γ = 0.5, with the rheological data from Γ = 0.5 from Fig. 2 overplotted in black.

hysteresis observed in the $\Omega(T)$ curves for the example of $\Gamma = 0.5$. We combine several torque-controlled data sets with the appropriate flow curve, and observe that while the precise location of individual hysteresis loops fluctuates, the characteristic torques remain confined to an interval which coincides well with the minimum and maximum of the $T(\Omega)$ curves. We concluded that for $\Gamma > 0$, hysteresis and negatively sloped flow curves are directly related.

Static yield vs dynamic yield for $\Gamma = 0$.—In the absence of vibrations, the connection between flow curves and instabilities is more subtle, as there is only one stable branch with a finite flow rate (although one could see the jammed state at small stress as the second ''stable branch''). We now ask the following question: when we slowly ramp up the torque, how is the resulting yielding behavior influenced by the nonmonotonic flow curve?

To answer, we study the statistics of static yielding by ramping up the applied torque at 0.5 mN m/s, fixing $\Gamma = 0$, and measuring the ensuing $\Omega(t)$. We identify a yield event whenever $\Omega > \Omega_{\mathrm{Th}} = 0.016$ rps. Our statistics are robust for Ω_{Th} between 0.002 and 0.13 rps, and over the duration of the experiment (~ 10 h), we do not observe any appreciable drift in the properties of the distribution. As indicated in Fig. 4(a), we observe two types of yielding: microyielding, where Ω only briefly peaks above Ω_{Th} (diamond), and global failure, where the increase in Ω is dramatic and persistent (square).

We measure the statistical properties of both types of yielding over 1943 torque ramps. In Fig. 4(b) we show the probability distribution functions of the microyielding torques (gray) and the global yielding torques (black). Consistent with the flow curve for $\Gamma = 0$ (Fig. 4(c)), we observe that microyield events do not occur above $T/T_d = 1$—once the torque is above the dynamic yield threshold, the material flows at a rate given by the positive slope region of the flow curve. What is surprising is that global yielding can happen both below and above T_d—invalidating the simple picture of a lower dynamic, and higher static yield threshold. Rather, the probability for complete failure is bounded by $T = T_{\mathrm{min}}$—for lower torques the flow curve shows there is no steady state flow, and only microyielding events are observed.

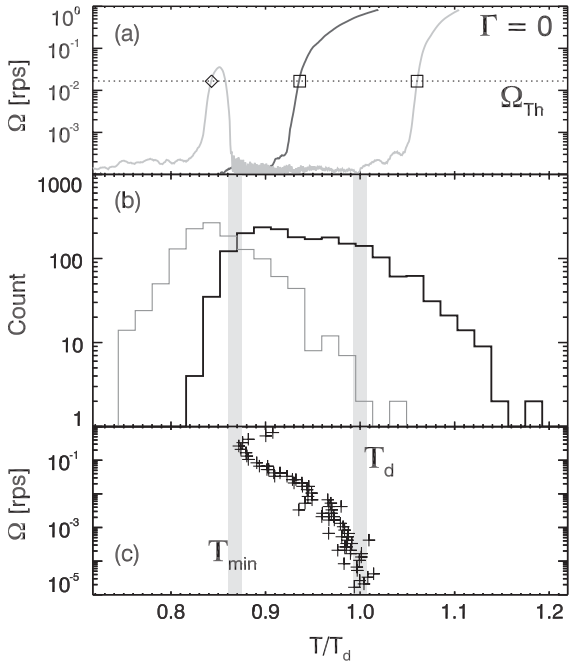

FIG. 4. (a) Typical examples of $\Omega(T)$ curves during a torque ramp. The dashed line indicates the threshold rotation rate $\Omega_{\mathrm{Th}} = 0.016$ rps that defines a yield event. ◇ indicates a microyielding event, □ a global failure event. (b) The probability distribution function of microyielding (gray) and global yielding (black). Gray bars indicate the onset value for the rheological instability T_{min}, and the dynamic yield stress T_d. (c) Flow curve for $\Gamma = 0$.

We conclude that, due to the nonmonotonic flow curve, there are three yielding regimes. Below T_{min}, microyielding without global yielding; above T_{min} but below T_d, microyielding with a finite probability of global yielding; above $T = T_d$ all yield events become global. This intermediate regime is clearly inconsistent with the simple picture where hysteresis in jamming and yielding of granular media is explained from the static threshold exceeding the dynamic one [Fig. 1(a)].

Robustness nonmonotonic flow curves.—How specific to the precise flow geometry and materials used are the nonmonotonic flow curves we observe? We test this in two ways. First, we can test the dependence of the rheology on the shape of the shear bands in the split-bottom cell itself with the glass beads mentioned earlier: for larger filling height, i.e., $H/R_s = 0.7$, the flow field is qualitatively very different [20–22]. We have conducted a series of experiments and we observe qualitatively the same flow curves and instabilities (not shown here).

Second, we probed the existence of the nonmonotonic flow curves for a range of materials in a standard vane geometry at $\Gamma = 0$. The top curve shown in Fig. 5 shows that the nonmonotonic flow curves for glass beads at $\Gamma = 0$ are not specific to the split-bottom geometry. However, details of the flow curves are material dependent—some materials (aluminum flakes and PMMA beads) do not have

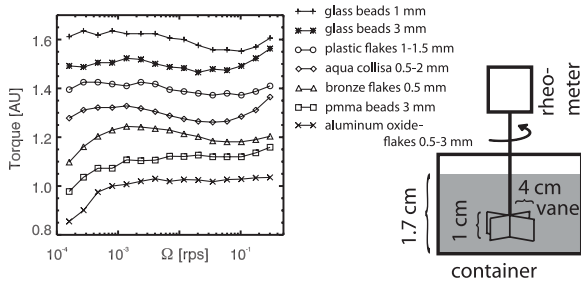

FIG. 5. Rheological curves for a range of materials as indicated, where a vane (see sketch) directly coupled to an Anton Paar MCR501 rheometer was placed just above the bottom. All torques are normalized by their mean value and (with the exception of the bottom curve) shifted upwards for clarity.

a negative slope at all, while others (bronze flakes, aqua collisa) have the positive-negative-positive slope combination that we saw above for $\Gamma > 0$ only. We do not know the cause of this material dependence, but suggest that material dependent plastic flow in the contact asperities may destroy the negative slope, and that for such materials, temperature may play a similar role as vibrations does for glass beads.

Conclusion.—We have shown that nonmonotonic flow curves are a robust feature of slow granular flows. As a consequence, the yielding transition at $\Gamma = 0$ exhibits all the hallmarks of a first order or subcritical transition. For finite Γ, the yield stress vanishes but the hysteretic nature of the transition persists up to a large value of Γ (around 1 for this filling height, somewhat smaller for larger H/R_s), where the transition becomes second order and smooth.

Our data suggest that material properties are key, and while we cannot exclude collective effects [25,26], a simple decrease of the particle-particle dynamic friction coefficient with rate may be sufficient [27]. Our findings provide crucial input for refining and extending current descriptions of granular flows [3,4].

J. A. D. acknowledges funding from the Dutch physics foundation FOM, and O. D. from the KNAW. We thank Bruno Andreotti, Bob Behringer, and Eric Clément for discussions and Jeroen Mesman for outstanding technical assistance in the construction of the rheological setup.

[1] J. Duran, *Sands, Powders and Grains: An Introduction to the Physics of Granular Materials* (Springer, New York, 1999).
[2] H. M. Jaeger, S. R. Nagel, and R. P. Behringer, Rev. Mod. Phys. **68**, 1259 (1996).
[3] GDR MiDi Collaboration, Eur. Phys. J. E **14**, 341 (2004).
[4] Y. Forterre and O. Pouliquen, Annu. Rev. Fluid Mech. **40**, 1 (2008).
[5] K. Nichol, A. Zanin, R. Bastien, E. Wandersman, and M. van Hecke, Phys. Rev. Lett. **104**, 078302 (2010).
[6] I. Sánchez *et al.*, Phys. Rev. E **76**, 060301 (2007).
[7] D. Rubin, N. Goldenson, and G. A. Voth, Phys. Rev. E **74**, 051307 (2006).
[8] H. M. Jaeger, C.-h. Liu, and S. R. Nagel, Phys. Rev. Lett. **62**, 40 (1989).
[9] P. Marchal, N. Smirani, and L. Choplin, J. Rheol. **53**, 1 (2009).
[10] A. Janda *et al.*, Europhys. Lett. **87**, 24002 (2009).
[11] K. A. Reddy, Y. Forterre, and O. Pouliquen, Phys. Rev. Lett. **106**, 108301 (2011).
[12] R. M. Nedderman and C. Laohakul, Powder Technol. **25**, 91 (1980).
[13] P. Coussot, *Rheometry of Pastes, Suspensions and Granular Materials* (John Wiley & Sons, Inc., Hoboken, New Jersey, 2005).
[14] F. Da Cruz, F. Chevoir, D. Bonn, and P. Coussot, Phys. Rev. E **66**, 051305 (2002).
[15] P. Mills, P. G. Rognon, and F. Chevoir, Europhys. Lett. **81**, 64005 (2008).
[16] H. M. Jaeger, C.-h Liu, S. R. Nagel, and T. A. Witten, Europhys. Lett. **11**, 619 (1990).
[17] J. D. Goddard, Annu. Rev. Fluid Mech. **35**, 113 (2003).
[18] L. Heymann and N. Aksel, Phys. Rev. E **75**, 021505 (2007).
[19] P. Schall and M. van Hecke, Annu. Rev. Fluid Mech. **42**, 67 (2010).
[20] D. Fenistein and M. van Hecke, Nature (London) **425**, 256 (2003); D. Fenistein, J.-W. van de Meent, and M. van Hecke, Phys. Rev. Lett. **92**, 094301 (2004); D. Fenistein, J.-W. van de Meent, and M. van Hecke, Phys. Rev. Lett. **96**, 118001 (2006); J. A. Dijksman and M. van Hecke, Soft Matter **6**, 2901 (2010).
[21] X. Cheng *et al.*, Phys. Rev. Lett. **96**, 038001 (2006).
[22] J. A. Dijksman *et al.*, Phys. Rev. E **82**, 060301 (2010).
[23] M. Depken *et al.*, Europhys. Lett. **78**, 58001 (2007).
[24] M. Pailha, M. Nicolas, and O. Pouliquen, Phys. Fluids **20**, 111701 (2008).
[25] R. R. Hartley and R. P. Behringer, Nature (London) **421**, 928 (2003).
[26] R. P. Behringer, D. Bi, B. Chakraborty, S. Henkes, and R. R. Hartley, Phys. Rev. Lett. **101**, 268301 (2008).
[27] T. Baumberger and C. Caroli, Adv. Phys. **55**, 279 (2006).